Systems/Circuits

# Laminar Dynamics of Target Selection in the Posterior Parietal Cortex of the Common Marmoset

Janahan Selvanayagam,[1,2] Kevin D. Johnston,[2,3] and Stefan Everling[1,2,3]

[1]Graduate Program in Neuroscience, Western University, London, Ontario N6A 3K7, Canada, [2]Center for Functional and Metabolic Mapping, Robarts Research Institute, Western University, London, Ontario N6A 3K7, Canada, and [3]Department of Physiology and Pharmacology, Western University, London, Ontario N6A 3K7, Canada

**The lateral intraparietal area (LIP) plays a crucial role in target selection and attention in primates, but the laminar microcircuitry of this region is largely unknown. To address this, we used ultra-high density laminar electrophysiology with Neuropixels probes to record neural activity in the posterior parietal cortex (PPC) of two adult marmosets while they performed a simple visual target selection task. Our results reveal neural correlates of visual target selection in the marmoset, similar to those observed in macaques and humans, with distinct timing and profiles of activity across cell types and cortical layers. Notably, a greater proportion of neurons exhibited stimulus-related activity in superficial layers whereas a greater proportion of infragranular neurons exhibited significant postsaccadic activity. Stimulus-related activity was first observed in granular layer putative interneurons, whereas target discrimination activity emerged first in supragranular layers putative pyramidal neurons, supporting a canonical laminar circuit underlying visual target selection in marmoset PPC. These findings provide novel insights into the neural basis of visual attention and target selection in primates.**

*Key words:* **laminar electrophysiology; lateral intraparietal area; marmoset; target selection; visual attention**

**Significance Statement**

**The lateral intraparietal area (LIP) is a critical cortical region for target selection and spatial attention. The microcircuitry of this region remains poorly understood as in the macaque, the most prevalent model, it is embedded within a sulcus and is inaccessible to laminar electrophysiological techniques. The common marmoset however is a promising alternative model due to its lissencephalic cortex and homologous frontoparietal network. Here, we conducted ultra-high density laminar electrophysiology in area LIP of marmosets performing a visual target selection task. We observed interlaminar dynamics consistent with previous observations of a canonical circuit in primary visual cortex and proposed models for the frontal eye fields, extending the concept of a canonical circuit to primate association cortex.**

## Introduction

At any given moment, we are faced with many more stimuli than can be processed simultaneously. To cope with this limitation, the process of attention acts to filter irrelevant stimuli and preferentially select those relevant for the guidance of behavior. In foveate animals such as primates, visual attention and eye movements are closely linked, and the neural mechanisms underlying these processes and their relation to one another have been a topic of intensive investigation. Convergent evidence from anatomical, lesion, fMRI, transcranial magnetic stimulation, and neurophysiological studies has demonstrated that attention and eye movements are supported by an extensively interconnected and largely overlapping network that includes the frontal eye fields (FEFs) within the prefrontal cortex, the lateral intraparietal area (LIP) within the posterior parietal cortex (PPC), and the midbrain superior colliculus (SC), an area critical for the generation of eye movements (see for review Johnston and Everling, 2008; McDowell et al., 2008).

The role of LIP in attentional and oculomotor control has been a topic of considerable interest, owing in part to its anatomical interposition between sensory and motor areas. LIP receives extensive inputs from multiple visual cortical areas, and as noted above is reciprocally interconnected with FEF and SC (Lynch et al., 1985; Andersen et al., 1990; Baizer et al., 1991;

Received Aug. 21, 2023; revised April 2, 2024; accepted April 6, 2024.

Author contributions: K.D.J. and S.E. designed research; J.S., K.D.J., and S.E. performed research; J.S. analyzed data.

We thank C. Vander Tuin, W. Froese, H. Pettypiece, and K. Faubert for expert technical and surgical assistance and care of the marmosets. This work was supported by the Canadian Institutes of Health Research grant FRN148365 and PJT183973 to S.E. and the Canada First Research Excellence Fund to BrainsCAN.

The authors declare no competing financial interests.

Correspondence should be addressed to Stefan Everling at severlin@uwo.ca.

https://doi.org/10.1523/JNEUROSCI.1583-23.2024

Schall, 1995; Lewis and Van Essen, 2000). As such, it has been conceptualized as a transitional link between visual processing and saccade generation. Consistent with this, single neurons in LIP have been shown to exhibit both visual and saccade-related responses (Andersen et al., 1987). More direct evidence has been provided by studies in macaque monkeys trained to perform variants of the visual search task, in which a target stimulus is selected from an array of distractors. Pharmacological inactivation of LIP has been shown to induce deficits in visual search performance (Wardak et al., 2002). Neurophysiological studies have revealed that the activity of LIP neurons evolves to discriminate targets from distractors presented within their response fields in advance of saccades to the target location (Ipata et al., 2006; Thomas and Paré, 2007; Mirpour et al., 2009) and that the time of this discrimination is predictive of the reaction times of targeting saccades (Thomas and Paré, 2007). Thus, the activity of LIP neurons may be said to instantiate a process of saccade target selection, in which an initial stage of visual selection is followed by activity related to the forthcoming saccade.

Broadly speaking, for tasks requiring target selection, the activity of LIP neurons resembles closely that of areas to which it projects. Neurons both in FEF (Thompson et al., 1996) and SC (McPeek and Keller, 2002; Shen et al., 2011) discriminate targets from distractor stimuli and discharge in advance of saccades. Although activity in both of these areas (Hanes and Schall, 1996; Dorris et al., 1997; Paré and Hanes, 2003) has been more directly linked to saccade initiation than that in LIP (Gottlieb and Goldberg, 1999), the considerable overlap in discharge properties across areas invites detailed investigations of the intrinsic mechanisms shaping the selection process within each area which in turn regulate the signals sent between them to fully understand their respective contributions to target selection. Anatomical and physiological evidence has demonstrated that area LIP possesses separate output channels to the FEF and SC. Corticocortical projections exhibit a visual bias and originate predominately in layers II/III, while corticofugal projections originate exclusively in layer V and exhibit a bias toward saccade-related activity (Lynch et al., 1985; Schall, 1995; Ferraina et al., 2002). To date, the laminar dynamics shaping these activity differences remain poorly understood, and although canonical circuit models have provided theoretical accounts with respect to visual cortex (Douglas and Martin, 1991) and the FEF (Heinzle et al., 2007), few studies have investigated directly the laminar flow of information by conducting simultaneous recordings across cortical layers (but see Godlove et al., 2014; Ninomiya et al., 2015; Nandy et al., 2017; Bastos et al., 2018; Pettine et al., 2019). The flow of neural activity in the primate PPC is unknown.

The lack of laminar recordings in frontoparietal networks is due in large part to the practical difficulty in accessing areas such as FEF and LIP in macaques due to their locations deep within sulci. In contrast, the common marmoset monkey (*Callithrix jacchus*) has a relatively lissencephalic cortex, making it well-suited for such investigations. Recent work has identified homologous regions to macaque and human FEF and LIP in marmosets using a variety of methods, including cyto- and myeloarchitectural features, anatomical connections, resting-state functional connectivity, task-based fMRI activations, intracortical microstimulation, and single-unit electrophysiology (Collins et al., 2005; Rosa et al., 2009; Reser et al., 2013; Ghahremani et al., 2017, 2019; Schaeffer et al., 2019; Selvanayagam et al., 2019; Ma et al., 2020; Feizpour et al., 2021). Here, we addressed the knowledge gap in the understanding of laminar dynamics and their role in instantiating the process of saccadic target selection by carrying out laminar electrophysiological recordings in the PPC of marmosets using ultra-high density Neuropixels probes (Jun et al., 2017) while they performed a simple visual target selection task in which they generated saccades to a target stimulus presented in either the presence or absence of a distractor. We observed neural correlates of visual target selection similar to those observed in macaques and humans, the timing of which varied across neuron type and cortical layer.

## Materials and Methods

*Subjects.* Two adult common marmosets (Marmoset M, female, age 22–24 months, weight 328–337 g; Marmoset N, male, age 23–35 months, weight 421–443 g) served as subjects in the present study. Prior to these experiments, both animals were acclimated to restraint in two separate custom-designed primate chairs for MRI and electrophysiological experiments which placed them in sphinx and upright positions, respectively. The animals additionally underwent an aseptic surgical procedure in which a combination recording chamber/head restraint was implanted, the purpose of which was to stabilize the head for MRI imaging, eye movement recording, and electrode insertions and to allow access to the cortex for electrophysiological recordings. These procedures have been described in detail previously (Johnston et al., 2018; Schaeffer et al., 2019). All experimental procedures were conducted in accordance with the Canadian Council on Animal Care policy on the care and use of laboratory animals and a protocol approved by the Animal Care Committee of the University of Western Ontario Council on Animal Care. The animals were additionally under the close supervision of university veterinarians throughout all experiments.

*Behavioral training.* For training on eye movement tasks, marmosets were seated in a custom primate chair (Johnston et al., 2018) inside a sound attenuating chamber (Crist Instrument), with the head restrained. A spout was placed at animals' mouth to allow delivery of a viscous liquid reward (acacia gum) via an infusion pump (Model NE-510, New Era Pump Systems). All visual stimuli were presented on a CRT monitor (ViewSonic Optiquest Q115, 76 Hz noninterlaced, 1,600 × 1,280 resolution) using either the CORTEX real-time operating system (NIMH) or MonkeyLogic (Hwang et al., 2019). Eye positions were digitally recorded at 1 kHz via infrared video tracking of the left pupil (EyeLink 1000, SR Research).

Marmosets were first trained to fixate on visual stimuli by rewarding 300–600 ms fixations within a circular electronic window with a diameter of 5° centered on circular stimuli consisting of dots with a diameter of 2° presented centrally on the display monitor. Once they were able to perform this subtask reliably, the number of potential fixation locations was increased with the addition of four stimuli presented at ±5° abscissa and ±5° ordinate. This served both as an initial training stage and allowed us to verify and adjust eye position calibration at the beginning of each experimental session.

Marmosets were then trained on the visual target selection task (Fig. 1*A*). This task consisted of two trial types. On "single-target" trials, the animals were required to generate a saccade to the location of a single peripheral visual stimulus in order to obtain a liquid reward. On each trial, they were required to maintain fixation within an electronic window with a diameter of 5° centered on a 0.5° dot presented at the center of the display monitor for a variable duration of 300–500 ms. Following this, a single-target stimulus, a marmoset face (3° diameter), was presented at ±6° abscissa. Animals were rewarded for single saccades to the target stimulus which landed within a circular electronic window of 5°, centered on the stimulus. Saccades landing elsewhere were marked as "incorrect." If no saccade was made within 1 s of target onset, the trial was marked as "no response." Once marmosets were consistently able to perform 100 or more correct trials of this task within a session, we added an additional "distractor" condition in which a distractor stimulus, a 1° radius black circle, was presented in the opposite hemifield at equal eccentricity to the target stimulus. All fixation and saccade requirements and the timing of trial events was identical to that of single-target trials. On distractor trials, single saccades to the target stimulus were rewarded

while those made to the distractor location were classified as errors. In the final version of the task the "single-target" and "distractor" conditions were run in alternating 20 trial blocks. Marmosets were trained on this task until they could complete 200 trials with at least 70% accuracy in the distractor blocks excluding "no response" trials. At this point we commenced collection of electrophysiological data. The final blocked version of the task including single-target and distractor conditions was used for all electrophysiological recording sessions.

*fMRI-based localization of recording locations.* To target LIP for electrophysiological recordings, we conducted an fMRI localizer prior to commencing electrophysiological recordings. To provide landmarks for the location of this area relative to the recording chamber and guide the placement of trephinations allowing access to cortex, a custom-designed in-house printed grid matched to the inside dimensions of the chamber, consisting of 1 mm holes at a spacing of 1.5 mm, was placed into the chamber, and the grid holes were filled with iodine solution prior to scanning. This allowed visualization of the chamber and grid coordinates in the MRI images. We then acquired awake anatomical T2 images from each animal and aligned these to a high-resolution ex vivo MRI template aligned with a group RS-fMRI functional connectivity map of the SC (https://www.marmosetbrainconnectome.org; Schaeffer et al., 2022). This group RS-fMRI map is based on over 70 h of RS-fMRI collected at ultra-high fields from 31 awake adult marmosets. Marmosets then underwent a second aseptic surgical procedure in which a microdrill (Foredom SR series, Blackstone Industries) was used to open burr holes of roughly 3 mm diameter over the region of the PPC identified as described above. This corresponded approximately to the stereotaxic location of 1.4 mm anterior, 6 mm lateral indicated for area LIP in the marmoset stereotaxic atlas of Paxinos et al. (2012) and explored in a previous microstimulation study in our lab (Ghahremani et al., 2019). As in that study, we were additionally able to visually identify a small blood vessel and shallow sulcus thought to be homologous to the intraparietal sulcus of macaque. The sites were then sealed with a silicone adhesive (Kwik-Sil, World Precision Instruments) which served to prevent infection and reduce growth of granulation tissue on the dural surface. This seal was removed prior to and replaced following recording sessions after thorough flushing and cleaning of the trephinations.

*Electrophysiological recordings.* Recordings were conducted using Neuropixels 1.0 NHP short probes (Jun et al., 2017). The external reference and ground were bridged in all recordings. All recordings were referenced to the reference contact at the tip of the electrode. Data were recorded in two streams, a spike stream sampled at 30 kHz and high-pass filtered at 300 Hz, and an local field potential (LFP) stream sampled at 2.5 kHz and low-pass filtered at 300 Hz. Custom Neuropixels electrode holders designed to interface with the dovetail structures on metal cap of the probe base were used with Narishige Stereotaxic Manipulators (SM-25A and SMM-200) to manipulate electrodes for all recordings. IMEC headstages were used with a PXIe-8381 acquisition module, and the PXIe-1082 chassis and the MXIe interface were used for data acquisition. Eight bit digital event signals emitted by CORTEX or MonkeyLogic and calibrated analog signals for the horizontal and vertical eye positions were recorded using the PXI-6133. Neural and auxiliary signals were synchronized by a transistor–transistor logic pulse emitted by CORTEX or MonkeyLogic at target onset. All data were acquired using the SpikeGLX application (v20190413-phase3B2; Karsh, 2019).

For each recording session, we removed the chamber cap and cleaned the recording chamber and dural surface to mitigate the risk of infection. First, we cleaned the outside of the chamber with sterile gauze soaked with 70% isopropyl alcohol solution. The silicone adhesive sealing the trephination was then removed and the dural surface was first flushed with sterile saline delivered via a syringe with a sterile catheter tip. Saline filling the chamber was absorbed with sterile gauze between flushing bouts. A 10% iodine solution was then applied, and the area was scrubbed extensively with sterile swabs. We then repeated saline flushing of the area until the solution appeared clear. Any blood or moisture on the dural surface was removed using absorbent surgical eye spears prior to electrode insertion, to avoid fouling of the electrode contacts. Probes were then advanced through the dura using stereotaxic micromanipulators until neural activity no longer appeared on the tip of the electrode where possible. Electrodes were allowed to settle for 30–45 min to minimize drift during the recording session. During this time, the animal's eye position was calibrated as described above. Then, animals performed the visual target selection task as described above until ∼50 correct trials were obtained in each of the conditions or 45 min had passed. Finally, a visual field mapping paradigm was conducted, in which 0.2° dots were briefly flashed (100–200 ms SOA, 0–100 ms ISI) in a pseudorandomized manner in an evenly spaced $5 \times 5$ grid spanning ±8° abscissa and ordinate. Animals were not required to fixate during this period, and trials where the eyes were closed or moved within ±200 ms of stimulus onset were removed from analysis offline.

In total, 26 penetrations were conducted across 22 sessions (8 in Marmoset M, 14 in Marmoset N), where 8 penetrations in Marmoset N were conducted with two Neuropixels probes simultaneously. For these penetrations, two probes were adhered back-to-back using dental adhesive (Bisco All-Bond, Bisco Dental Products) and advanced together using a single electrode holder.

*Semiautomated spike sorting.* Data collected in the spike stream were additionally high-pass filtered offline at 300 Hz. Putative single-unit clusters were then extracted using Kilosort 2 (Pachitariu et al., 2023). Briefly, a common median filter is applied across channels, and a "whitening" filter is applied to reduce correlations between channels and maximize local differences among nearby channels. Following these preprocessing steps, templates are constructed based on some initial segment of the data and adapted throughout session with some accommodation for drift over time. Then clusters are separated and merged as necessary.

Following this process, putative single-unit clusters were manually curated using the Phy application (Rossant, 2019). Here, clusters were merged or split on the basis of waveforms, cross-correlations, and distributions of spike amplitudes. Following merging and splitting clusters as needed, clusters with consistent waveforms, normally distributed amplitudes, a dip in the autocorrelogram at time 0, and consistently observed throughout the recording session were marked as single units, and all others were marked as multiunit clusters or noise clusters as appropriate. Single-unit clusters where the firing rate across the session was at least 0.5 Hz and at most 1% of interspike intervals (ISIs) were within 1 ms (i.e., short ISIs that fall within the refractory period) were retained for all subsequent analyses. For these neurons, short ISI spikes were discarded.

*Layer assignment based on spectrolaminar LFP analysis.* Layer assignment was done as in previous work, using an established spectrolaminar pattern (Mendoza-Halliday et al., 2023). Powerline artifacts were removed at 60 Hz using a butterworth bandstop filter. As these recordings were referenced to the tip of the electrode, as compared with the surface reference used in the recordings of Mendoza-Halliday et al. (2023), to recover the pattern they observed, we subtracted the mean activity in channels visually identified as being above the surface from all other channels. Then, the LFP activity aligned to stimulus onset was extracted and the power spectral density (PSD) was computed for each trial using the multitaper method (Mitra and Pesaran, 1999). This was then averaged across tapers and trials to obtain the mean PSD for a given penetration. The PSD of adjacent channels was then averaged to obtain the mean PSD at each depth (Fig. 2*D*,*E*). Following visual inspection, power in the 15–22 Hz range was used for the low-frequency range and 80–150 Hz was used for the high-frequency range. The crossing point in the power of these ranges across depth was marked as the center of layer IV. Upon visual inspection of the density of neurons anchored to this point and the known thickness of layer IV in marmoset PPC, we assigned neurons found from 200 µm below this point to 300 µm above as being in layer IV. Neurons superficial to this range were assigned to layers II/III and those found deeper to layers V/VI.

*Putative cell-type classification using peak–trough widths.* We clustered neurons as broad and narrow spiking (BS and NS) cells on the basis of peak–trough width, which has been suggested to correspond to

putative pyramidal cells and interneurons, respectively (McCormick et al., 1985; Mitchell et al., 2007; Hussar and Pasternak, 2012; Ardid et al., 2015). For each neuron, the channel at which the spike amplitude had the largest magnitude was selected. The mean waveform at this channel was upsampled to 1 MHz and interpolated using a cubic spline. For cells where the largest amplitude was a peak, that is, positive-first waveforms, we identified a nearby channel with a negative-first waveform as the estimated depth of the soma and discarded neurons for which such a waveform could not be identified. For the retained neurons, the large and well-isolated positive-first waveform was inverted to ensure that all waveforms exhibited a negative-going pattern and the peak–trough duration could be estimated reliably. Then, the duration between this trough and the subsequent peak were computed as the peak–trough widths (Fig. 2*F*). Neurons with a peak–trough width >300 ms were classified as BS and those with a peak–trough width smaller than 300 ms were classified as NS.

*Identification of task modulated and target discriminating neurons.* Neurons were classified as task modulated if activity 40 ms from stimulus onset to 25 ms after saccade offset significantly differed from baseline activity (200 ms prior to stimulus onset) on contralateral "single-target" trials or "distractor" trials. Significance was assessed using paired samples *t* tests for each neuron at an α level of 0.05. For these neurons, activity in the 50 ms interval preceding saccade onset was correlated with saccade reaction times (SRTs) for contralateral and ipsilateral "single-target" trials via Pearson's *r* correlations at an α level of 0.05. Neurons were classified as target discriminating if activity 50–100 ms following stimulus onset significantly differed ipsilateral and contralateral "distractor" trials. Significance was assessed using independent samples *t* tests for each neuron at an α level of 0.05. Neurons were classified as postsaccadic if the activity 50–150 ms following saccade offset differed from the prestimulus baseline separately for each condition and across all conditions using paired samples *t* tests for each neuron at an α level of 0.05. For all above neurons, we conducted receiver operating characteristics (ROC) analyses (Green and Swets, 1966) comparing the distributions of discharge activity in 15 ms sliding windows to determine the onset times of the observed effects. Significance was determined by comparing to a null distribution constructed via permutation testing using 1,000 iterations. We evaluated differences in the proportions of neurons with significant stimulus-related, discrimination, or postsaccadic activity (i.e., epoch) across layers and cell types using a logistic regression analysis: $P \sim \text{epoch} * \text{layer} * \text{cell-type}$ (lme4::glmer v1.1-31 in R v4.2.2). Model significance was estimated by comparison using likelihood ratio chi-squared test with reduced models excluding each of these terms. Pairwise differences were computed using Bonferroni's corrections (emmeans v1.8.4 in R).

*Assessing differences in the timing of stimulus-related and discrimination activity across layers and putative cell classes.* To assess the contribution of neurons from different cortical layers and putative cell classes to the stimulus-related and discrimination activity across the population, we employed a generalized additive model (GAM). Here, the odds of a spike at a given point in time are estimated using the time from stimulus onset and depth relative to the crossing point described above (as a tensor product smooth predictor), and putative cell class (NS or BS), with trial and neuron as random effects: $P \sim \text{te}(\text{time} * \text{depth}, \text{by} = \text{celltype} * \text{condition}) + (\text{time}|\text{trial}) + (\text{time}|\text{neuron})$; (mgcv:bam v1.8-41 in R). That is, a two-dimensional spline function is evaluated over time and depth, where the parameters of these functions vary for the cell classes and conditions. Spiking odds over time are allowed to vary randomly across neurons and trials. For the stimulus-related activity condition (ipsilateral and contralateral was added as a predictor. For the discrimination activity, condition (preferred and nonpreferred) was added as a predictor, where, for each neuron, the stimulus (target or distractor) which elicited the greatest discharge activity was labeled as preferred. Goodness of fit of models as compared with reduced and null models was assessed using the likelihood ratio chi-squared test. Pairwise differences were examined by estimating difference smooths, that is, smooth functions corresponding to the difference between levels of a categorical predictor interacting with the time by depth tensor product smooths. The time where significant stimulus-related activity first emerged was computed by determining where the 99.9% CI of the difference smooth between ipsilateral and contralateral trials for the "single-target" condition deviated from 0. Similarly, to determine the time at which neurons first significantly discriminated between target and distractor stimuli, we determined where the 99.9% CI of the difference smooth between preferred and nonpreferred trials for the "distractor" condition deviated from 0.

## Results

### Behavioral performance

Marmosets performed visually guided saccades in a simple target selection task wherein blocks of "single-target" and "distractor" trials were presented to the animal (Fig. 1*A*). Animals were

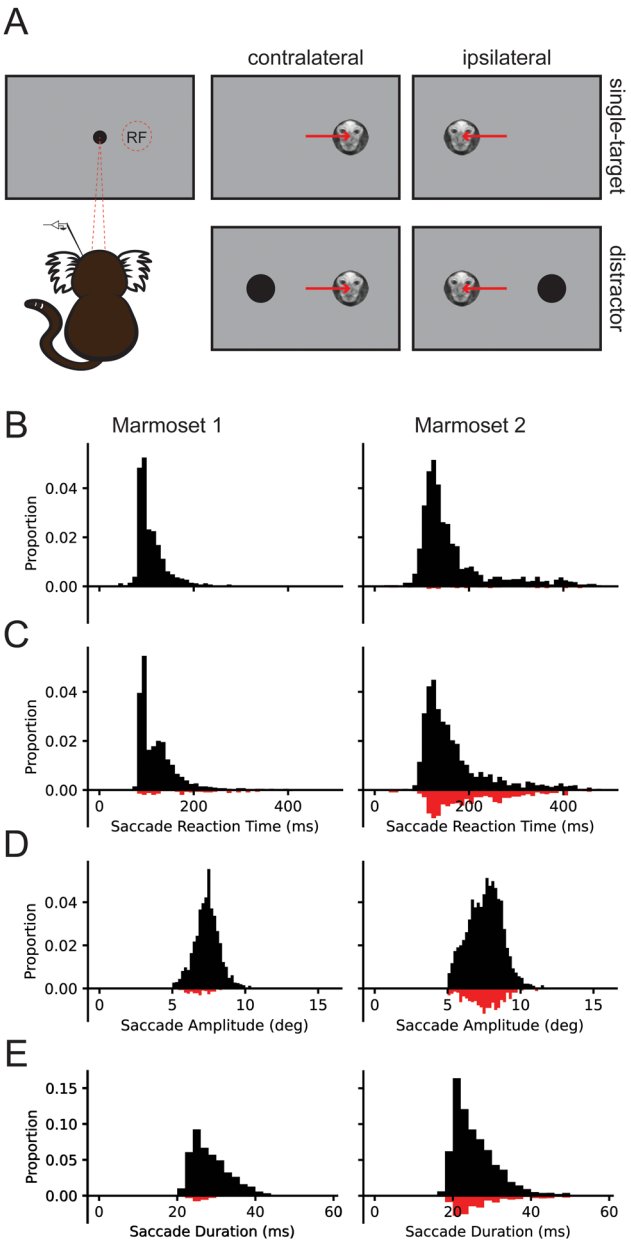


**Figure 1.** Task design and behavioral performance. ***A***, Schematic representing task design for "single-target" and "distractor" trials, where the target falls in (contralateral) or out of (ipsilateral) the receptive field (RF). Saccade metrics for Marmoset 1 (left) and Marmoset 2 (right) for correct (black) and error (red) trials. SRT histograms for "single-target" (***B***) and "distractor" (***C***) trials for each animal separately. Saccade amplitude (***D***) and duration (***E***) histograms for each animal separately across all conditions.

required to fixate on a central fixation stimulus (0.5° radius black circle on a gray background) for 300–500 ms at the beginning of each trial. On "single-target" trials, a single target (1° diameter image of a marmoset face) was presented 6° to the left or right of the fixation stimulus, and subjects were required to make a saccade to the target to obtain a viscous liquid reward of acacia gum. On "distractor" trials, a distractor stimulus (0.5° radius black circle) was simultaneously presented in the opposite hemifield. Trials in which no saccade at least 4° in amplitude was made were marked as "no response" and were not included in further analysis. Trials in which saccades were made to the target were marked as correct and trials in which saccades landed anywhere else were marked as incorrect. We conducted 22 recording sessions, 8 in Marmoset M and 14 in Marmoset N, in which animals performed 162–438 trials ($M = 248.7$ trials). Accuracy was significantly lower on "distractor" trials (mean ± SEM; Marmoset M, 89.9 ± 2.2%; Marmoset N, 74.0 ± 4.0%; Fig. 1*C*) than on "single-target" trials (Marmoset M, 100.0 ± 0.0%; Marmoset N, 96.4 ± 0.5%; Fig. 1*B*), Marmoset M: $t_{(7)} = 4.57$, $p = 0.003$, Marmoset N: $t_{(13)} = 5.82$, $p < 0.001$; and median SRTs were significantly longer, Marmoset M: $t_{(7)} = 3.29$, $p = 0.013$, Marmoset N: $t_{(13)} = 3.79$, $p = 0.002$ (Marmoset M: "distractor" = 110.0 ± 4.0 ms vs "single-target" = 99.4 ± 1.6 ms; Marmoset N: "distractor" = 146.8 ± 6.5 ms vs "single-target" = 139.0 ± 5.2 ms). Saccade amplitude and durations did not differ significantly between conditions nor on correct vs incorrect trials (all $p$'s > 0.05; Fig. 1*D*,*E*). Taken together, these results reveal a distractor-induced reduction in performance suggesting an additional stage of processing on these trials.

### Determining recording locations, cortical layers, and putative neuron classes

To determine recording locations, we acquired high-resolution, anatomical T2 images from each animal. Prior to scanning, a custom-designed grid with 1.5 mm diameter holes spaced at 1 mm was inserted in the animals' recording chambers and filled with iodine solution. The filled grid holes provided landmarks for determining the locations of identified areas within the recording chamber. We then aligned these images to a high-resolution ex vivo MRI template (REF?) aligned with a group RS-fMRI functional connectivity map of the SC (https://www.marmosetbrainconnectome.org; Schaeffer et al., 2022). We identified a region of strong functional connectivity in the PPC corresponding to the location of area LIP (Fig. 2*A*–*C*; Ghahremani et al., 2019; Schaeffer et al., 2019). Marmosets subsequently underwent aseptic surgeries in which we opened trephinations of ∼3 mm in diameter over this region.

We conducted 26 electrode penetrations in two animals (Marmoset M: 8 penetrations in 8 sessions; Marmoset N: 18 penetrations in 14 sessions) in which we advanced either one or two Neuropixels electrodes (Jun et al., 2017) in this region and recorded the activity of 1,366 well-isolated single neurons. For each penetration, we determined cortical layers by identifying the crossover point between the PSD of low (15–22 Hz) and high (80–150 Hz) frequency ranges in the LFPs across depths as done in previous work (Mendoza-Halliday et al., 2023; Fig. 2*D*,*E*). Based on visual inspection of the distribution of isolated neurons distributed along the length of the electrode shank, and the known density of neuronal distributions within the cortical layers in this region of marmoset cortex, we classified all neurons that fell within 200 μm below to 300 μm above as being in granular layer IV and all others as supragranular or infragranular. To classify putative interneurons and pyramidal cells, the established approach of using the peak–trough duration was employed (McCormick et al., 1985; Mitchell et al., 2007; Hussar and Pasternak, 2012; Ardid et al., 2015; Fig. 2*F*). Interestingly, a large proportion of neurons with positive-first waveforms were observed (198%, 14.5%), which were largely restricted to the broad waveforms observed in deeper layers. For 90 of these neurons, we were able to identify a nearby or deeper channel, where we observed a negative-first waveform, and for these neurons we reassigned the relative depths accordingly (Fig. 2*F*, white circles). For the remaining 108 neurons, we were unable to identify a negative-first waveform, in part due to very small amplitudes or the neuron being clipped by the spatial extent of the probe. As these waveforms may also correspond to axons corresponding to a soma in a superficial layer, we excluded these neurons from the analysis. For the neurons we retained, we inverted the positive-first waveform before evaluating the peak–trough duration, as often the negative-first waveform was of a small amplitude and may lead to poor estimates of peak–trough duration.

### Evaluating stimulus and saccade-related responses in LIP neurons

To identify task-modulated neurons, we computed the mean discharge rates from 50 ms after stimulus onset to 25 ms after saccade onset for conditions and compared it with the mean baseline activity 200 ms before stimulus onset. Examining the conditions separately, 333 (24.15%) neurons were significantly modulated in the "single-target" contralateral condition as compared with 115 (8.34%) in the "single-target" ipsilateral condition; for the "distractor" trials, 322 (23.35%) were significantly modulated when the target was presented in the contralateral hemifield as compared with 253 (18.35%) when the distractor was presented in the contralateral hemifield. Overall, pooling across conditions, a total of 381 (27.63%) neurons exhibited significant modulations in discharge rates during task performance (Fig. 3). The proportion of modulated neurons per layer and putative cell class were as follows (Table 1): supragranular (BS, 28.18%; NS, 37.04%), granular (BS, 26.82%; NS, 27.61%), and infragranular (BS, 17.12%; NS, 21.59%).

For these neurons, we conducted Pearson's $r$ correlations to determine whether activity preceding saccade onset correlated with the SRTs for contralateral and ipsilateral trials separately; the discharge activity of 32 (8.2%) and 33 (8.5%) neurons were significantly correlated with SRTs ($p$'s < 0.05), respectively, suggesting there may be little correspondence between the activity of these neurons and the motor planning of the upcoming saccades.

For these neurons, to examine the evolution of stimulus-related activity over time, we conducted ROC analyses (Green and Swets, 1966) comparing the distributions of discharge activity following stimulus onset as compared with a prestimulus baseline interval. We computed auROC values on discharge rates within successive 15 ms intervals from stimulus onset to 200 ms after stimulus onset as compared with 200 ms before stimulus onset. To evaluate the significance of auROC values, we compared these values to a null distribution created by shuffling the labels of baseline versus stimulus-related 1,000 times at each interval. For each neuron, we determined the first time point where a significant auROC value was observed and determined cumulative distributions for each layer (Fig. 4*A*). No significant differences were observed between layers for the onset of stimulus-related activity.

We then compared the activity of these neurons in the same interval on distractor trials in which the target was in the

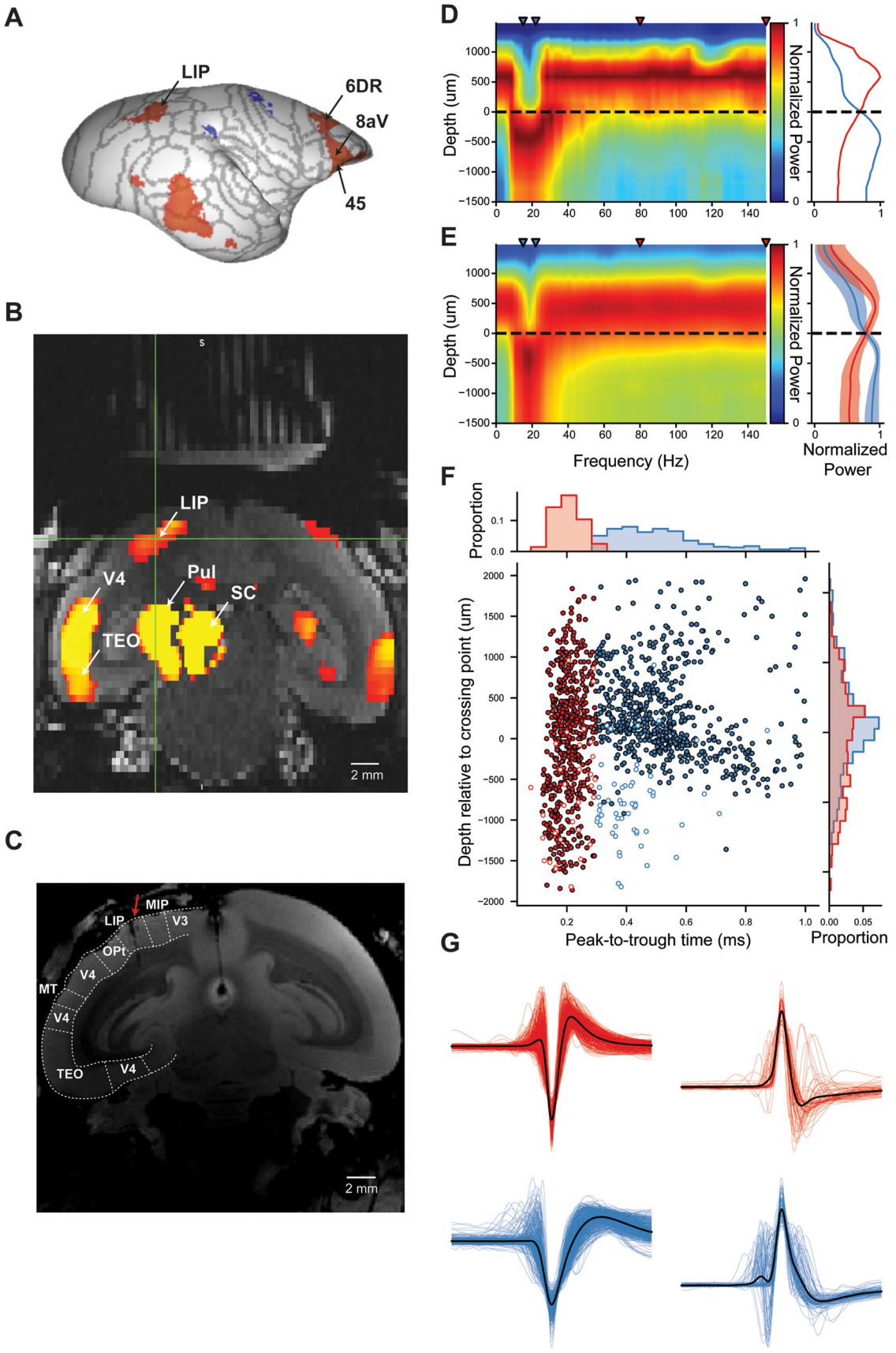


**Figure 2.** Localization of recording locations, layer assignment and cell-type classification. ***A***, Surface map of RS-fMRI functional connectivity (FC) with the SC to identify LIP. ***B***, Coronal slice of anatomical MRI of Marmoset M with an overlay of FC maps from ***A*** interpolated to native space of Marmoset M to identify location of LIP relative to the grid. ***C***, Ex vivo anatomical MRI of Marmoset N with Paxinos et al. (2012) boundaries overlaid confirming electrode tract locations (as indicated by red arrow) in LIP. LFP power aligned to stimulus onset across depths and frequencies (left) and normalized power in selected ranges (right; blue, 15–22 Hz; red, 80–150 Hz) are shown for an example session (***D***) and the average of all sessions (***E***). The crossing

contralateral or ipsilateral hemifield. One-hundred and sixty-eight (12.3%) neurons significantly discriminated between targets and distractor presented in the contralateral hemifield, of which 135 (80% of discriminating neurons) showed greater activity for the target stimulus (Fig. 5, Table 1): supragranular (BS, 9.28%; NS, 14.40%), granular (BS, 16.09%; NS, 16.42%), and infragranular (BS, 7.21%; NS, 10.13%).

For these neurons, to assess the magnitude and timing of the discrimination activity, we conducted auROC analyses comparing the distributions of activity on the trials in which the preferred (i.e., the stimulus with the greater mean discharge activity in the task epoch) or nonpreferred stimulus was presented in the contralateral hemifield. We computed auROC values on discharge rates within successive 15 ms intervals from stimulus onset to 200 ms after stimulus onset. As with the stimulus-related activity, we compared the auROC values with null distributions for each neuron at each time point and determined the discrimination times for each neuron and evaluated cumulative distributions for each layer (Fig. 4*B*). We also determined the magnitude and time from stimulus onset of the maximal auROC value for each neuron. Medians across layers and putative cell class were as follows: supragranular (BS: 0.296, 98 ms; NS: 0.581, 92 ms), granular (BS: 0.599, 99 ms; NS: 0.615, 109 ms), and infragranular (BS: 0.581, 86 ms; NS: 0.577, 88 ms). Notably, the maximal auROC values were generally observed before the median SRTs; however, the timing and magnitude of the discrimination did not differ appreciably between layers and cell types.

We additionally observed a large proportion of neurons that displayed strong postsaccadic modulations in activity across conditions. Generally, this activity started at saccade offset, peaked ~50–100 ms later and often persisted for 300–500 ms. To identify neurons with significant postsaccadic activity, we computed the mean discharge rates from 50 to 150 ms after saccade offset where we observed the peak of the activity and compared it with the 200 ms prestimulus baseline used above, separately for each condition. For correct trials, 969 neurons (70.94%) had significant postsaccadic activity in at least one condition, 688 neurons in at least two conditions, 391 in at least three conditions, 203 in all four conditions, and 551–581 neurons for each condition (Fig. 6). Postsaccadic activity did not appear to correspond with stimulus-related activity; of the 329 neurons with significant stimulus-related activity in the contralateral "single-target" condition, 58 neurons had significant postsaccadic activity in the ipsilateral "single-target" condition, 71 in the contralateral and 101 in both. For the "distractor" conditions, we examined postsaccadic activity on error trials and observed that only half the number of neurons had significant postsaccadic activity (ipsilateral, 231 neurons as compared with 551, 119 neurons in both; contralateral, 288 neurons as compared with 566, 165 in both). In sum, a large proportion of neurons exhibited postsaccadic activity, and this activity varied depending on stimulus identity and task performance.

To examine how this activity evolves over time, we conducted auROC analyses for each neuron, comparing the distributions of discharge activity in 15 ms steps from saccade onset for 200 ms to a 50 ms presaccadic baseline. As we did not have specific predictions about laminar or cell-type differences regarding this activity, we computed the cumulative distribution of significant auROC values across all neurons, separately for each condition (Fig. 4*C*). We observed that many of the neurons exhibited significant increases in discharge activity 25–75 ms following saccade onset (~50 ms from saccade offset), which would be too early for stimulus-related activity in response to stimuli at the saccade landing position. However, many neurons did respond after 75 ms from saccade onset, and some of these neurons may possess perifoveal receptive fields. Notably, postsaccadic increases in discharge activity were observed significantly later, $F_{(1,177)} = 9.81$, $p = 0.002$, in the ipsilateral single-target condition ($M = 121.3$ ms) compared with all three other conditions ($M = 101$–$103$ ms), further suggesting this activity may not be strictly related to stimulus-related properties following saccade offset but rather reflect the target selection and saccade processes pertaining to those saccades.

For comparison with the above, we determined the proportion of neurons with significant postsaccadic activity across conditions. We then conducted a logistic regression to investigate the effects of layer, cell type, and epoch (task, discrimination, postsaccadic) on the likelihood that a neuron has significantly different discharge activity. This model explained significantly more variance than the reduced two-way models ($p < 0.05$) and revealed that NS infragranular neurons were less likely to be significantly modulated in the task interval and BS infragranular neurons were less likely to significantly discriminate between target and distractor but were more likely to have significant postsaccadic activity as compared with respective granular and supragranular layer neurons ($p$'s $< 0.05$; Table 1).

Regarding infragranular layer neurons, it can be difficult to ascertain the boundary between layer 6 and the white matter. Indeed, trailing cell bodies can be observed in the white matter alongside many axons. As such, it is possible some of the neurons labeled here as originating in the infragranular layers may be axons corresponding to more superficial neurons. To investigate this possibility, we repeated the above single neuron analyses while excluding the 258 neurons below −700 μm from the labeled crossing point. With this conservative approach, we observed that the proportions of significant neurons were largely similar. Indeed, we observed that infragranular layer neurons were still less likely to significantly discriminate between target and distractor stimuli than supragranular and granular layer neurons. However, we did not observe greater proportions of neurons with postsaccadic activity in infragranular layers as compared with granular and supragranular layers. Further investigation is required to determine the nature of saccade-related activity of infragranular LIP neurons. Taken together with our exclusion of neurons with positive-first waveforms with no identifiable corresponding negative-first waveform at a nearby depth, we argue that the spike waveforms observed here can be attributed to infragranular layer neurons and not to axons.

In sum, we observed in marmosets LIP neurons which were significantly modulated in a visual target selection task and, in particular, those that discriminated between target and distractor stimuli before making a saccade. Further, this activity was observed across cortical laminae and cell types, albeit in slightly

←

point between lower and higher frequencies is marked by a dotted line. Peak-to-trough times for all recorded neurons across depth relative to the crossing point described above (***F***) and example waveforms of "broad" and "narrow" waveforms (***G***). Note that neurons for which we observed a positive-first waveform ($N = 198$) are identified by white circles in ***F*** and plotted separately in ***G***. LIP, lateral intraparietal area; MIP, medial intraparietal area; TEO, temporal area TE occipital part; MT, middle temporal area; Opt, occipitoparietal transitional area.

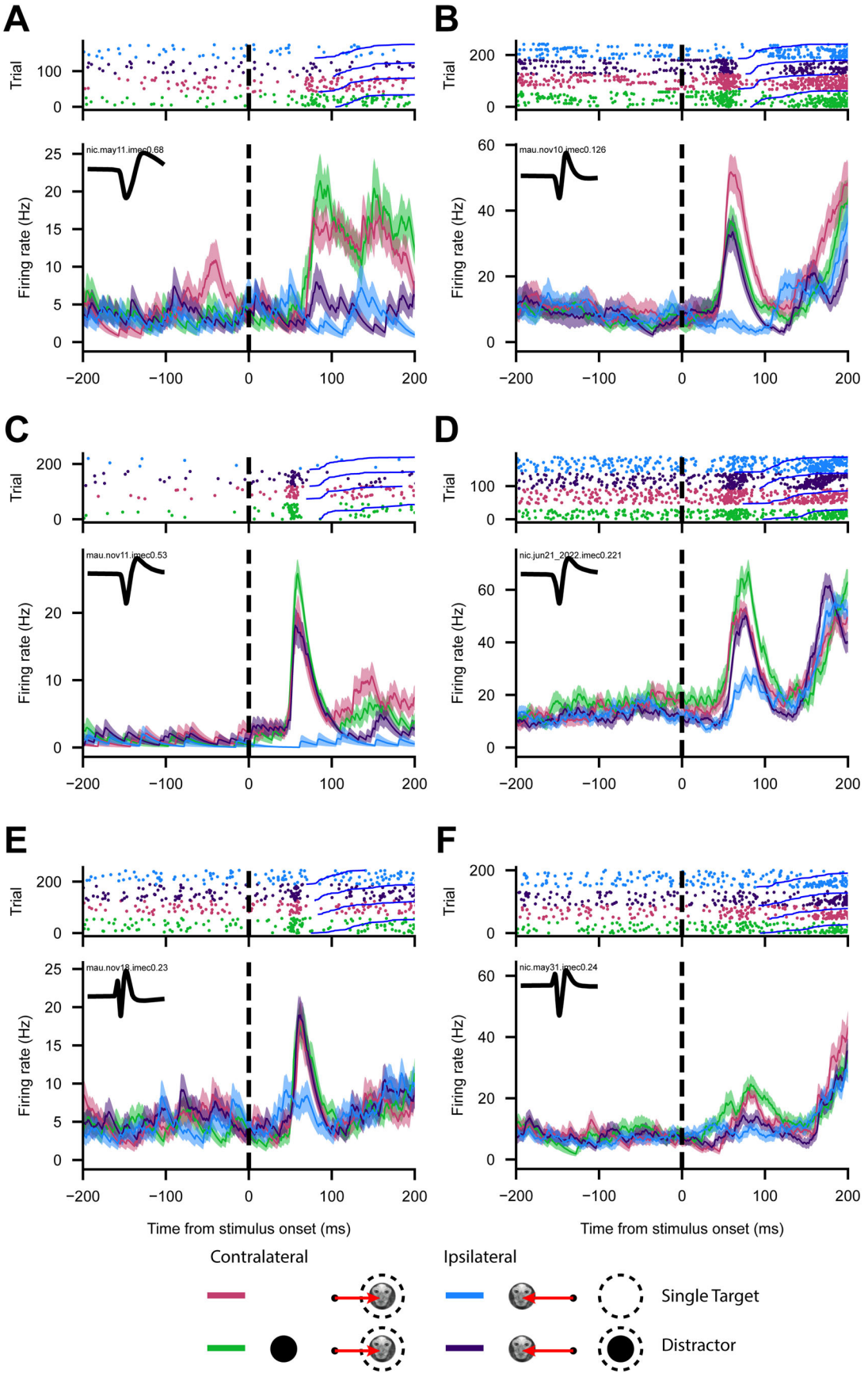


**Figure 3.** Example visual neurons. Raster plots and spike density functions (SDFs) aligned to stimulus onset, for example, broad-spiking (***A***,***C***,***E***) and narrow-spiking (***B***,***D***,***F***) neurons from supragranular (***A***,***B***), granular (***C***,***D***) and infragranular (***E***,***F***) layers with visual activity. Red, target contralateral; green, target contralateral and distractor ipsilateral; blue, target ipsilateral; purple, target ipsilateral and distractor contralateral. Blue lines in raster plot represent saccade onset. Trials are sorted into conditions and in order of increasing SRTs in raster plots. Mean waveform in inset SDF figure. Shaded regions in SDF figures represent ±1 SEM for each condition.

different proportions; supragranular and granular neurons were more likely to demonstrate stimulus- and target selection-related activity whereas infragranular neurons were more likely to have significant postsaccadic activity.

### Stimulus-related activity first emerges in NS granular layer neurons

To examine if and how the emergence of stimulus-related activity differs across cortical layers and cell types, we investigated the population activity using GAMs. GAMs are a type of statistical model which fits data to a "smooth" curve composed of many line segments by estimating the value at each "knot," the boundaries of these segments (Hastie and Tibshirani, 1986). In this manner, GAMs can capture complex, nonlinear relationships such as how neural activity varies over time (Cadarso-Suarez et al., 2006). Here, for the entire population of recorded neurons, we modeled the odds of a spike at each point in time and depth as a function of time from stimulus onset (ms), relative depth from the crossing point of low and high frequency power (μm), and cell type (BS, NS) for the contralateral and ipsilateral "single-target" condition. We employed a traditional stepwise regression approach for model selection wherein we constructed reduced models which successively excluded the factors of cell type, depth, condition, and time as well as the random effects of neuron and trial. We then compared these models using the chi-squared likelihood ratio test. This model significantly improved fit as compared with the reduced models ($p < 0.001$). As the vast majority of neurons only exhibited significant increases in discharge activity for contralateral as compared with ipsilateral "single-target" trials, we could evaluate the onset of stimulus-related activity by comparing the activity between these conditions. To examine differences between these conditions across time and depth, we may compute estimates of the pairwise differences between conditions for the time by depth tensor smooths separately for BS and NS neuron populations. Points in time and depth where these difference smooths deviate significantly from zero (evaluated here at a 99.9% CI) are where the conditions significantly differ. As such, we can determine the earliest time point and depths where stimulus-related activity was first observed for each cell type (Figs. 7, 8). The earliest stimulus-related activity first emerges in narrow-spiking neurons 0–500 μm below the crossing point 35 ms following stimulus onset, followed by more superficial narrow-spiking and broad-spiking neurons 38–40 ms following stimulus onset, likely corresponding to granular and supragranular neurons, respectively (Fig. 7). For ease of exposition, the model was discretized across depth into supragranular, granular, and infragranular layers as was done for the single neuron analyses above (Fig. 8). Stimulus-related activity first emerged in NS granular and supragranular neurons (36 ms), followed by BS supragranular neurons (39 ms) and finally in BS granular layer neurons (40 ms). Excluding neurons below −700 μm did not change the time points at which the earliest significant differences were observed. In sum, this suggests that stimulus-related activity first emerges in the granular layer and then in supragranular layers and occurs first in NS, that is, putative interneurons. The population stimulus-related activity in infragranular layers did not reach significance at any time point.

**Table 1. Description**

| Layer | Cell type | Stimulus-related | Discrimination | Postsaccadic |
|---|---|---|---|---|
| Infragranular | NS | 49 (21.58%) | 23 (10.13%) | 137 (60.35%) |
| | BS | 19 (17.11%) | 8 (7.20%) | 71 (63.96%) |
| Granular | NS | 37 (27.61%) | 22 (16.41%) | 83 (61.94%) |
| | BS | 70 (26.81%) | 42 (16.09%) | 147 (56.32%) |
| Supragranular | NS | 90 (37.03%) | 35 (14.40%) | 151 (62.13%) |
| | BS | 82 (28.17%) | 27 (9.27%) | 181 (62.19%) |

### Target discrimination-related activity first emerges in BS supragranular neurons

Next, we examined how target discrimination activity first emerges in the population activity using a GAM where we modeled odds of spiking using time, depth, cell type, and condition (ipsilateral vs contralateral "distractor" trials; $p < 0.05$). We then computed difference smooths between the conditions with a 99.9% CI, identified time points where this difference smooth deviated from 0 (Fig. 7), and determined the earliest time point and depths where target discrimination activity was observed for each cell type. The earliest discrimination activity was observed in broad-spiking neurons 1,000 μm above the crossing point 56 ms after stimulus onset, followed by broad-spiking and narrow-spiking neurons around the crossing point 58–65 ms after stimulus onset. As above, when using discrete layer

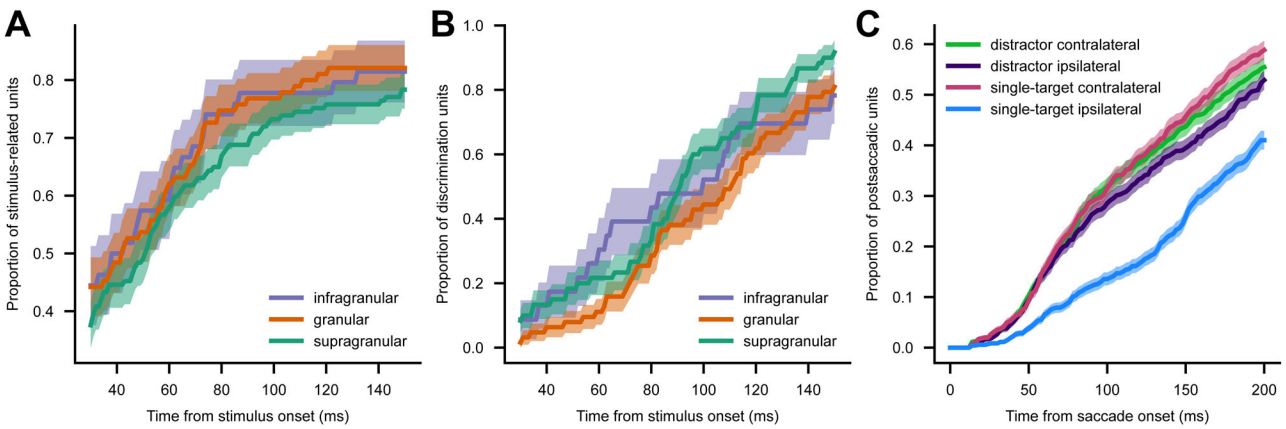


**Figure 4.** ROC analyses for stimulus and saccade-related activity. Cumulative distributions of neurons over time with significant auROC as compared with a null distribution generated from 1,000 randomized shuffles. ***A***, Significant stimulus-related activity as compared with a prestimulus baseline in single-target contralateral over time from stimulus onset separately for each cortical layer. ***B***, Significant target discriminating activity comparing ipsilateral and contralateral distractor trials over time from stimulus onset separately for each cortical layer. ***C***, Significant postsaccadic activity comparing each condition separately to a presaccadic baseline over time from saccade onset. Shaded region indicates 95% CI.

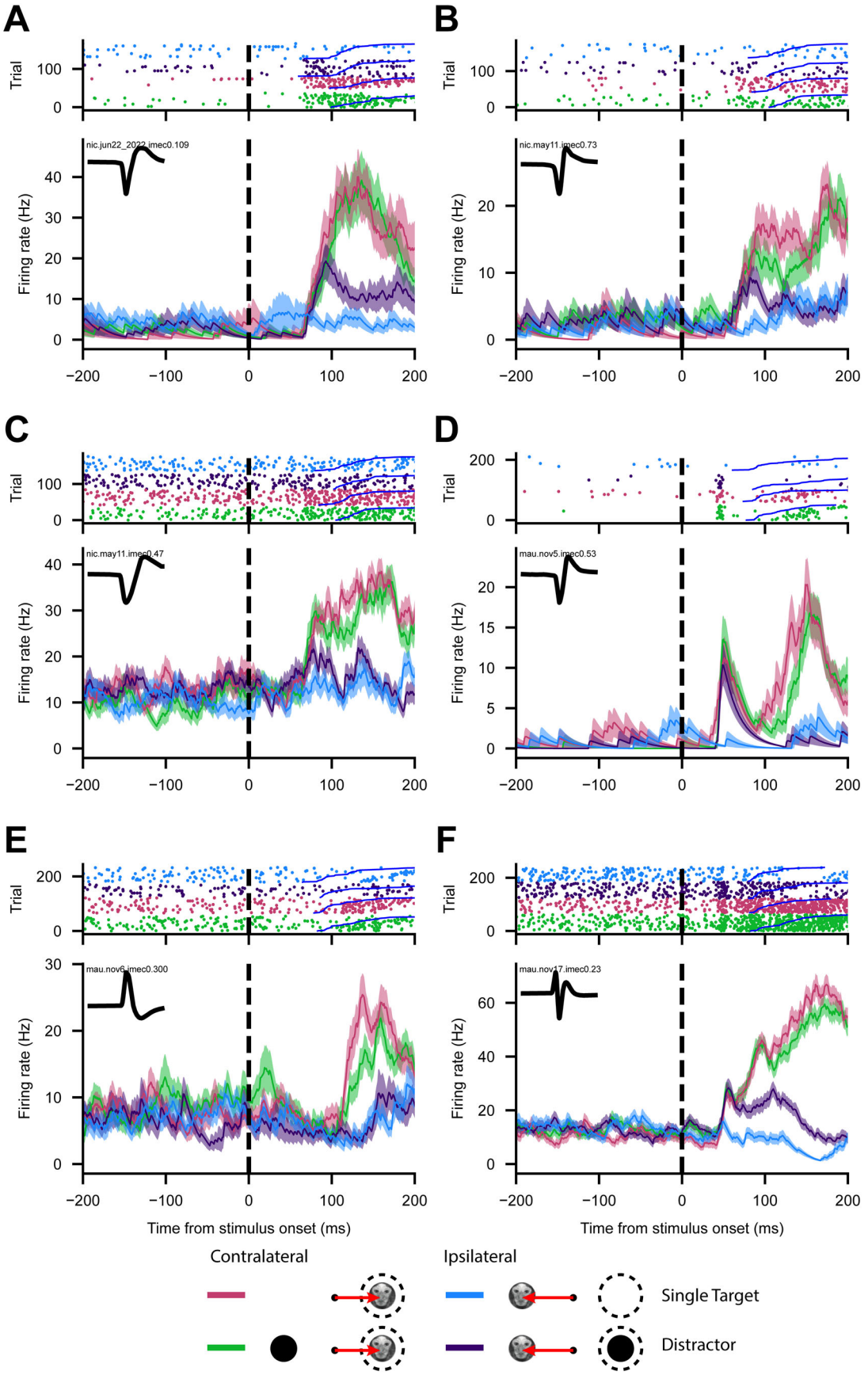


**Figure 5.** Example target discriminating neurons. Raster plots and spike density functions (SDFs) aligned to stimulus onset, for example, broad-spiking (***A***,***C***,***E***) and narrow-spiking (***B***,***D***,***F***) neurons from supragranular (***A***,***B***), granular (***C***,***D***), and infragranular (***E***,***F***) layers with activity discriminating between target and distractor stimuli. Red, target contralateral; green, target contralateral and distractor ipsilateral; blue, target ipsilateral; purple, target ipsilateral and distractor contralateral. Blue lines in raster plot represent saccade onset. Trials are sorted into conditions and in order of increasing SRTs in raster plots. Mean waveform in inset SDF figure. Shaded regions in SDF figures represent ±1 SEM for each condition.

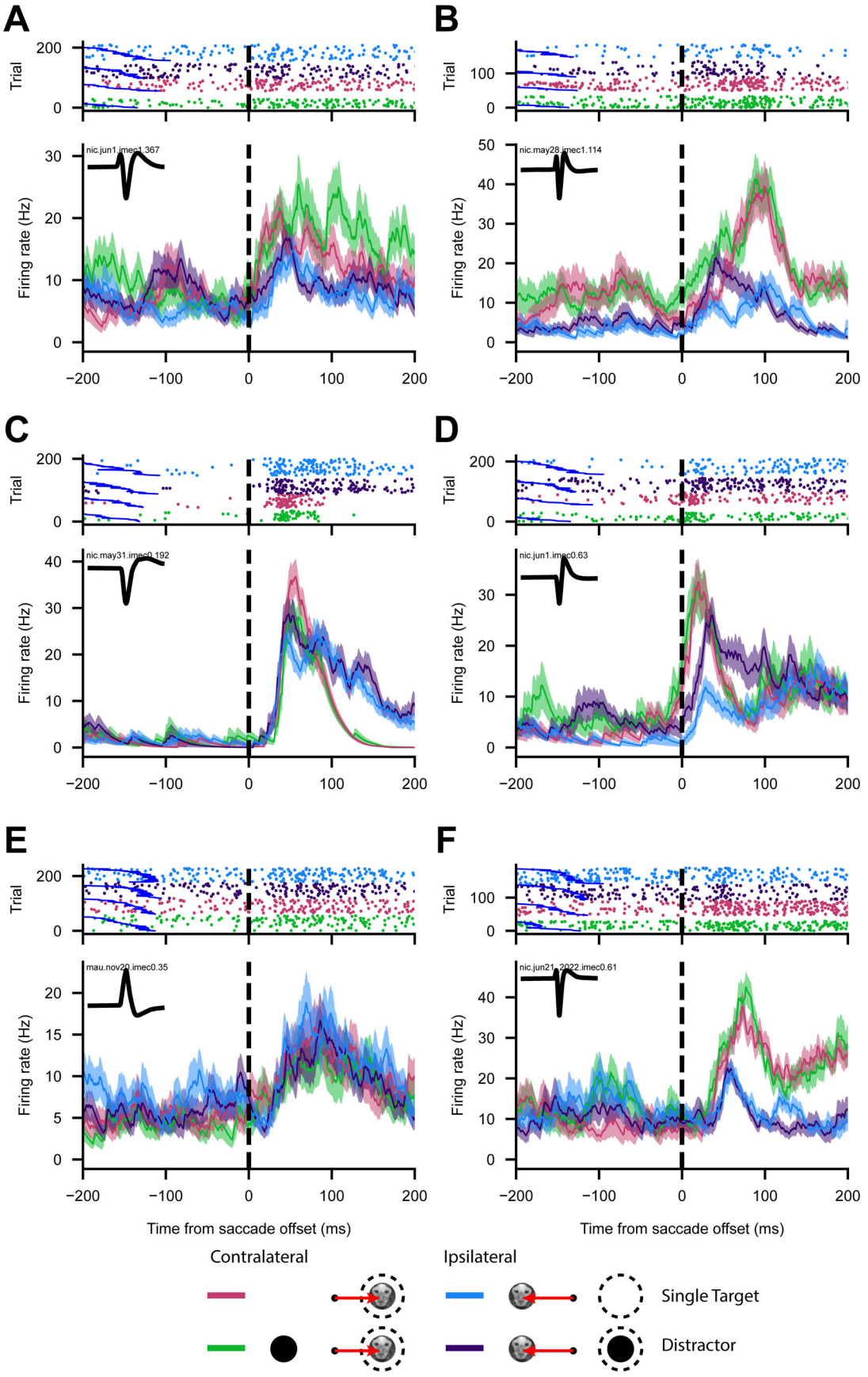


**Figure 6.** Example postsaccadic neurons. Raster plots and spike density functions (SDFs) aligned to saccade offset, for example, broad-spiking (***A***,***C***,***E***) and narrow-spiking (***B***,***D***,***F***) neurons from supragranular (***A***,***B***), granular (***C***,***D***) and infragranular (***E***,***F***) layers with significant postsaccadic activity. Red, target contralateral; green, target contralateral and distractor ipsilateral; blue, target ipsilateral; purple, target ipsilateral and distractor contralateral. Blue lines in raster plot represent saccade onset. Trials are sorted into conditions and in order of increasing SRTs in raster plots. Mean waveform in inset SDF figure. Shaded regions in SDF figures represent ±1 SEM for each condition.

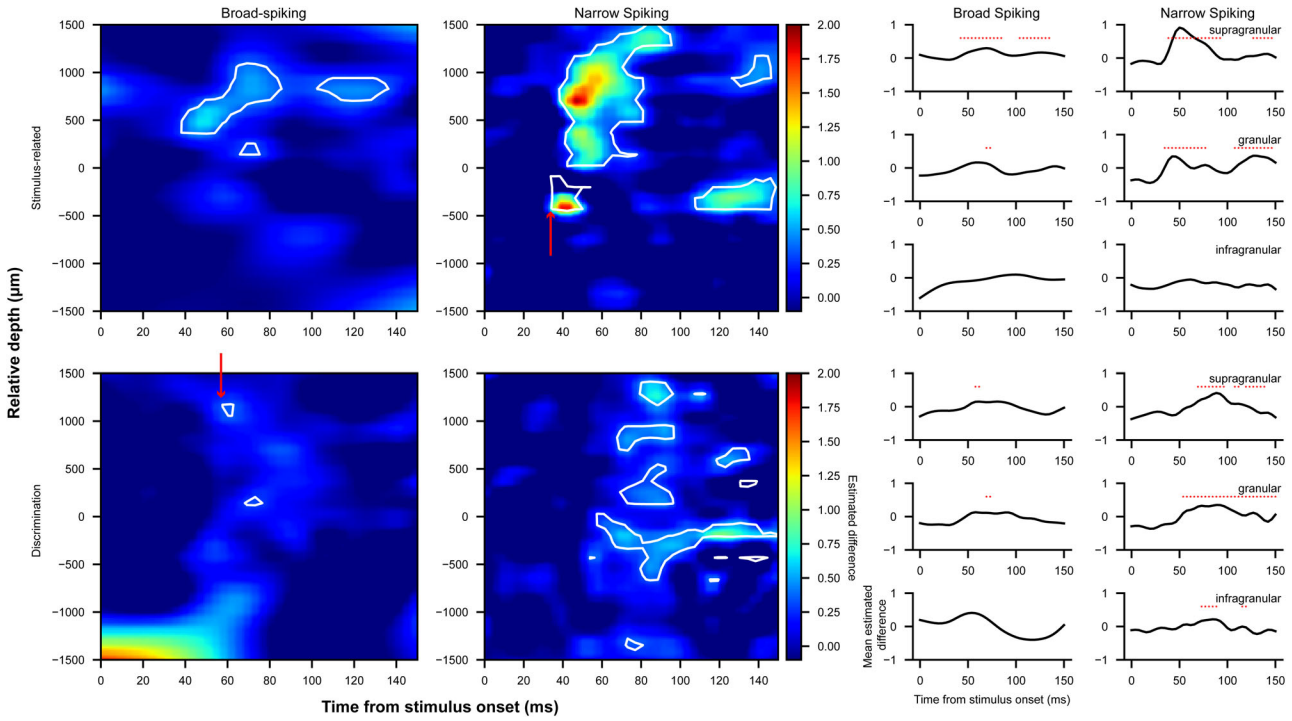


**Figure 7.** GAM fit of population activity continuously across depth. Odds of a spike at a given point in time are estimated using the time from stimulus onset, the relative depth from the crossing point, putative cell class (NS or BS), and the condition of the given trial (stimulus-related, ipsilateral vs contralateral single-target trials; discrimination, preferred vs nonpreferred distractor trials) with trial and neuron as random effects. Estimated differences across depth and time are plotted separately for stimulus-related (top) and discrimination (bottom), broad-spiking (left) and narrow-spiking (right) as heatmaps, with significant differences between conditions as determined by a 99.9% CI highlighted in white contours. Mean difference traces across depth ranges roughly corresponding to cortical layers are plotted on the right, separately for comparison and cell type. Significant differences are indicated by red *.

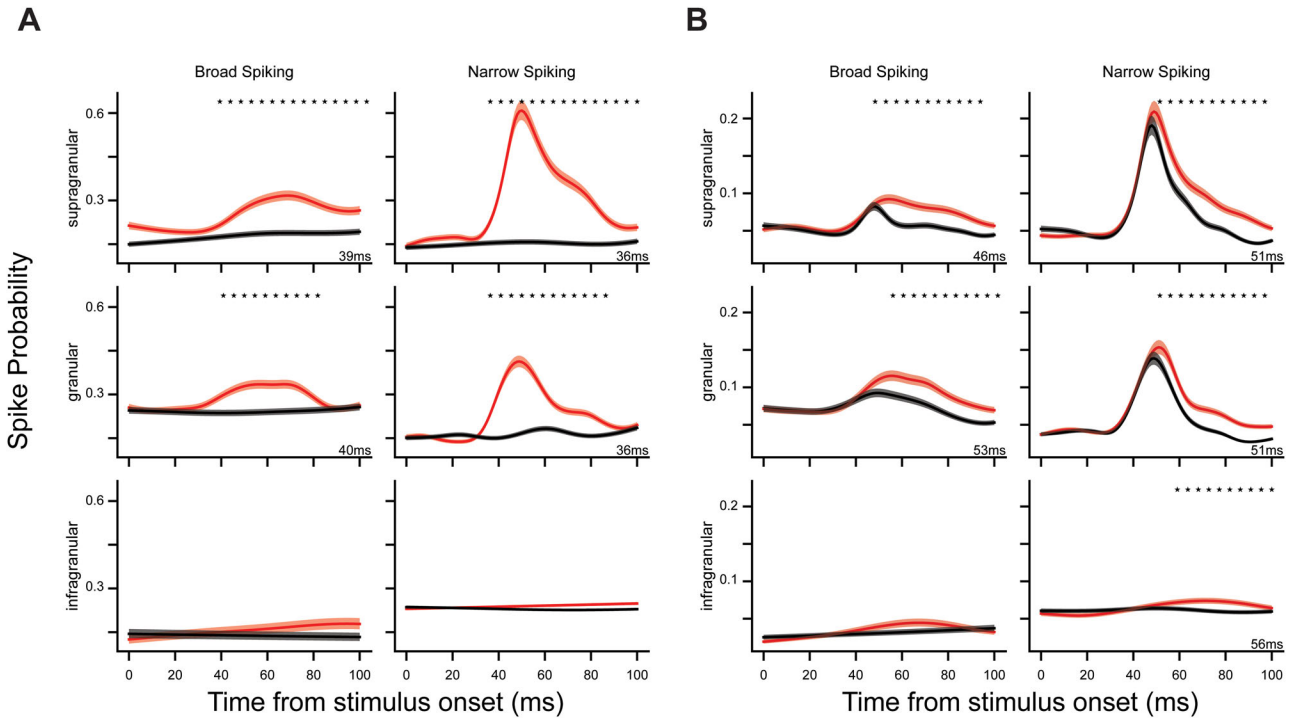


**Figure 8.** GAM fit for population stimulus-related and discrimination activity separately for layers. ***A***, Odds of a spike at a given point in time are estimated using the time from stimulus onset, the putative layer the neuron is found in (supragranular, granular, or infragranular), putative cell class (NS or BS), and the condition of the given trial ("single-target" ipsilateral or contralateral) with trial and neuron as random effects. Spike probability in the ipsilateral (black) and contralateral (red) conditions are plotted here for broad-spiking (left) and narrow-spiking (right) neurons for supragranular, granular, and infragranular layers. ***B***, Odds of a spike at a given point in time are estimated using the time from stimulus onset, the putative layer the neuron is found in (supragranular, granular, or infragranular), putative cell class (NS or BS), and the condition of the given trial ("distractor" preferred vs nonpreferred) with trial and neuron as random effects. Spike probability in the preferred (red) and nonpreferred (black) conditions are plotted here for broad-spiking (left) and narrow-spiking (right) neurons for supragranular, granular, and infragranular layers. *significant difference between conditions at 99.9% CI. First significant time point noted in bottom right corner in millisecond. Shaded region indicates ±1 SEM.

categories across depth (Fig. 8): we observed target discrimination activity first in BS supragranular neurons (46 ms), followed by narrow-spiking granular and supragranular neurons (51 ms), then in BS granular layer neurons (53 ms), and finally in NS infragranular layer neurons (56 ms). Excluding neurons below −700 μm did not change the time points at which the earliest significant differences were observed. Altogether, we see target discrimination emerges rapidly in superficial layers and predominantly in BS neurons.

In sum, although neurons with stimulus-related and target discrimination activity were observed across cortical laminae, subtle differences in the timing of this activity were observed at the population level, suggesting the granular layer as the primary input and supragranular layers as the first to discriminate between targets and distractors.

## Discussion

The laminar microcircuitry underlying visual target selection and saccade control in PPC remains poorly understood due to limitations of previously used animal models and experimental approaches. Here, we employed ultra-high density laminar electrophysiology in the PPC of common marmosets as they completed a saccadic target selection task to address this gap. As expected, we observed neurons with stimulus-related activity and, for the first time in the marmoset, neurons that discriminated between target and distractor stimuli. The stimulus-related activity observed here first emerged in the granular layer, followed by supragranular layers, with population activity in infragranular layers never reaching significance. This activity emerged first in putative interneurons followed by putative pyramidal neurons. Conversely, activity discriminating between target and distractor stimuli first emerged in supragranular neurons, followed by infragranular and finally granular layers, usually first appearing in putative pyramidal neurons. Altogether, the observed patterns support the existence of a canonical circuit consistent with previous models (Douglas and Martin, 2004; Heinzle et al., 2007).

Since its first description in Andersen et al. (1987) and Barash et al. (1991a,b), LIP has been the focus of intensive investigation for its role in the control of visual attention and eye movements. Single neuron recordings in macaque LIP have demonstrated that neurons in this area respond selectively to relevant visual stimuli and are critical in guiding visual attention and saccadic eye movements (Andersen et al., 1987; Gnadt and Andersen, 1988; Barash et al., 1991a,b; Colby et al., 1996; Kusunoki et al., 2000). Subsequent work, typically employing variants of the visual search task, has demonstrated activity in LIP which evolves to discriminate the presence of targets or distractors within their response fields (Ipata et al., 2006; Thomas and Paré, 2007; Mirpour et al., 2009). Investigations using pharmacological interventions and cortical cooling have further demonstrated a causal role for LIP in regulating visual salience (Wardak et al., 2002; Chen et al., 2020). Consistent with these observations, for the first time in the common marmoset, we observed a number of neurons that in a simple target selection task, responded to visual stimuli, a large proportion of which discriminated targets from distractors. Further, this discrimination activity generally peaked in advance of the upcoming saccade to the target location, consistent with a visual selection process preceding saccade generation. However, for these neurons, the magnitude of the discharge activity preceding the saccade did not correlate with the SRTs, though this is not surprising as the activity of LIP neurons does not strictly predict the motor plan underlying upcoming saccadic eye movements but rather represents the current locus of attention across the visual field (Kusunoki et al., 2000; Goldberg et al., 2002; Bisley and Goldberg, 2003; Bisley et al., 2011).

Surprisingly, a large proportion of neurons displayed significant postsaccadic activity across conditions which began immediately after saccade offset and often persisted up to 500 ms. As this activity is observed for both ipsilateral and contralateral trials in the "single-target" condition, it is unlikely to reflect remapping signals for a stimulus passing through the future receptive field of a neuron, as is observed in LIP neurons for "double-step" saccade paradigms (Duhamel et al., 1992). While it is possible that for some neurons this activity could be explained by stimulus-related activity for the target stimulus in a perifoveal receptive field at saccade offset, this is unlikely to be the sole source of this activity as for many neurons this activity is observed immediately following saccade offset. Additionally, the onset of this activity is delayed in the single-target ipsilateral trials and is observed in fewer neurons, despite the same perifoveal visual input. This activity could reflect the efference copy of the saccade, that is, corollary discharge (Sommer and Wurtz, 2008). In FEF, corollary discharge activity can be observed which is relayed from SC by the medial dorsal nucleus of the thalamus (Sommer and Wurtz, 2004, 2006). The observed activity here could be corollary discharge activity from SC in a similar pathway through pulvinar or from FEF. It has been previously observed that this activity in PPC can reflect saccadic error or saccade duration (Zhou et al., 2016, 2018; Munuera and Duhamel, 2020). It is worth noting that for many of these neurons, this activity varied across conditions and as a function of task performance while saccade amplitude and duration did not, suggesting this activity is not merely an efference copy but may encode other task-relevant variables.

While the activity of LIP neurons has not been shown to be tightly linked to saccade initiation, such activity can be observed in other frontoparietal structures such as FEF and SC with which LIP is strongly interconnected. Notably, LIP projections to these areas are largely segregated within distinct cortical laminae; corticocortical projections originate primarily in supragranular layers II/III and tend to convey visual information whereas corticotectal projections originate exclusively from infragranular layer V and primarily carry saccade-related information (Lynch et al., 1985; Schall, 1995; Ferraina et al., 2002). Indeed, computational models based on studies of macaque FEF and observed laminar circuits in cat primary visual cortex (Douglas and Martin, 2004; Heinzle et al., 2007) propose layer IV as the input, layers II/III as being responsible for the rule-based allocation of attention, and layer V as the primary output. These observations motivate investigations of laminar dynamics of areas such as FEF and LIP underlying these differences. Although these are challenging to pursue in the macaque due to the location of these areas in sulci prohibiting laminar electrophysiology, the lissencephalic cortex of the marmoset lends itself well to such investigations.

To this end, we used established methods of identifying cortical layers based on the PSD (Mendoza-Halliday et al., 2023) and classifying putative cell classes on the basis of peak–trough widths (McCormick et al., 1985; Mitchell et al., 2007; Hussar and Pasternak, 2012; Ardid et al., 2015). We reliably observed a crossing point in the power of low and high frequencies across depths, indicative of granular layer IV, from which we were able to separate the cortex into supragranular, granular, and infragranular layers. Regarding cell-type classification, we observed a larger than expected proportion of positive–negative

waveforms, which were largely restricted to BS infragranular neurons. These waveforms likely correspond to spikes recorded at the apical dendritic trunk of pyramidal neurons with large apical dendritic arbors which may be more commonly encountered in deeper layers (Boulton et al., 1990, p. 9). For many of these neurons, we observed lower-amplitude, negative–positive waveforms on deeper electrode contacts consistent with spikes recorded at the soma. To classify these neurons, we simply inverted the waveform before computing the peak–trough width. Notably, many of the neurons with large positive-first waveforms were observed at deeper sites. To examine the possibility that the spike waveforms observed for the deepest neurons actually correspond to axons of more superficial neurons, we excluded the deepest neurons and repeated our analyses. We observed little difference in either the proportions of neurons with task-modulated activity or the timing of these activity patterns. As such, we retained these neurons for all analyses.

We then assessed how the observed activity varied across cortical laminae and putative cell classes. First, we examined the proportion of neurons with significant stimulus-related, discrimination, and postsaccadic activity. NS supragranular/granular layer neurons were more likely to have stimulus-related activity as compared with infragranular neurons. Similarly, superficial BS neurons were more likely to discriminate between targets and distractors. Conversely, BS infragranular neurons were more likely than their superficial counterparts to display significant postsaccadic activity. These observations are consistent with the proposed role of superficial layers in visual input and attentional deployment and deeper layers for output.

Interestingly, we observed no difference in the maximal magnitude of the discrimination between target and distractor stimuli across layers or putative cell classes. However, the timing of how this activity evolves did differ. We first observed stimulus-related activity in putative interneurons in the granular layer followed by supragranular layer neurons. This is consistent with what is observed in other cortical areas and proposed by theoretical models. Moreover, this is consistent with the anatomy as corticocortical feedforward projections and thalamic input primarily terminate in granular layer IV and to a lesser extent, supragranular layers (Baizer et al., 1991; Matsuzaki et al., 2004). That it is observed first in putative interneurons as compared with pyramidal neurons is perhaps surprising as the primary target of long-range cortical projections are spiny neurons, which are generally pyramidal neurons (Anderson et al., 2011). However, this is characteristic of thalamocortical feedforward inhibition as observed in mouse barrel cortex (Swadlow, 2002). Here it is observed that monosynaptic thalamocortical input to somata of broadly tuned and highly sensitive layer IV interneurons act to rapidly drive inhibition which in turn sharpens the tuning properties of nearby pyramidal cells. Next, also consistent with our hypothesis, we observed discrimination between target and distractor stimuli first in putative pyramidal neurons in supragranular layers. Neurons in this layer are known to share reciprocal projections other key cortical structures involved in visual target selection such as FEF (Ferraina et al., 2002).

In sum, we identified single neurons exhibiting stimulus-related activity and those that discriminate between target and distractor stimuli across all layers and cell types albeit at different proportions and times. These observations are consistent with observations in single neuron investigations of LIP. Ferraina et al. (2002) antidromically identified populations of LIP neurons that were either a more superficial corticocortical, FEF-projecting population, or a deeper corticotectal, SC-projecting population. While these populations did possess similar stimulus-related, delay, and saccade-related activity, a greater proportion of the more superficial corticocortical population exhibited stimulus-related activity whereas a greater proportion of the deeper corticotectal population exhibited delay and saccade-related activity. These observations are consistent with our own, highlighting a role of more superficial neurons in earlier visual processing and deeper neurons in later saccadic stages. This can also be observed in FEF, where layer V corticotectal neurons represent activity at nearly all stages of visuomotor processing but tended to be more related to movement than more superficial corticocortical neurons (Everling and Munoz, 2000; Wurtz et al., 2001). Similarly in V4, a greater proportion of neurons with visual activity and feature selectivity can be observed in superficial layers as compared with a greater representation of eye movement-related signals in deeper layers (Pettine et al., 2019; Westerberg et al., 2021).

Altogether, our findings demonstrate single neuron target selection-related activity in the PPC of marmoset monkeys. Critically, we found interlaminar dynamics underlying this activity in primate association cortex consistent with a "canonical circuit" resembling that observed in primary visual cortex and proposed for the FEFs. These dynamics are characterized by a flow of neural activity from granular, to supragranular, to infragranular layers, with stimulus-related activity emerging first in granular layer putative interneurons and target discrimination first emerging in supragranular putative pyramidal neurons.

## References

Andersen RA, Bracewell RM, Barash S, Gnadt J, Fogassi L (1990) Eye position effects on visual, memory, and saccade-related activity in areas LIP and 7a of macaque. J Neurosci 10:1176–1196.

Andersen RA, Essick GK, Siegel RM (1987) Neurons of area 7 activated by both visual stimuli and oculomotor behavior. Exp Brain Res 67: 316–322.

Anderson JC, Kennedy H, Martin KAC (2011) Pathways of attention: synaptic relationships of frontal eye field to V4, lateral intraparietal cortex, and area 46 in macaque monkey. J Neurosci 31:10872–10881.

Ardid S, Vinck M, Kaping D, Marquez S, Everling S, Womelsdorf T (2015) Mapping of functionally characterized cell classes onto canonical circuit operations in primate prefrontal cortex. J Neurosci 35:2975–2991.

Baizer J, Ungerleider L, Desimone R (1991) Organization of visual inputs to the inferior temporal and posterior parietal cortex in macaques. J Neurosci 11:168–190.

Barash S, Bracewell RM, Fogassi L, Gnadt JW, Andersen RA (1991a) Saccade-related activity in the lateral intraparietal area. I. Temporal properties; comparison with area 7a. J Neurophysiol 66:1095–1108.

Barash S, Bracewell RM, Fogassi L, Gnadt JW, Andersen RA (1991b) Saccade-related activity in the lateral intraparietal area. II. Spatial properties. J Neurophysiol 66:1109–1124.

Bastos AM, Loonis R, Kornblith S, Lundqvist M, Miller EK (2018) Laminar recordings in frontal cortex suggest distinct layers for maintenance and control of working memory. Proc Natl Acad Sci U S A 115:1117–1122.

Bisley JW, Goldberg ME (2003) Neuronal activity in the lateral intraparietal area and spatial attention. Science 299:81–86.

Bisley JW, Mirpour K, Arcizet F, Ong WS (2011) The role of the lateral intraparietal area in orienting attention and its implications for visual search. Eur J Neurosci 33:1982–1990.

Boulton AA, Baker GB, Vanderwolf CH (1990) *Neurophysiological techniques, II (Vol. 15)*. Clifton, NJ: Humana Press.

Cadarso-Suarez C, Roca-Pardinas J, Molenberghs G, Faes C, Nacher V, Ojeda S, Acuna C (2006) Flexible modelling of neuron firing rates across different experimental conditions: an application to neural activity in the prefrontal cortex during a discrimination task. J R Stat Soc C Appl Stat 55: 431–447.

Chen X, Zirnsak M, Vega GM, Govil E, Lomber SG, Moore T (2020) Parietal cortex regulates visual salience and salience-driven behavior. Neuron 106: 177–187.e4.

Colby CL, Duhamel J-R, Goldberg ME (1996) Visual, presaccadic, and cognitive activation of single neurons in monkey lateral intraparietal area. J Neurophysiol 76:2841–2852.
Collins CE, Lyon DC, Kaas JH (2005) Distribution across cortical areas of neurons projecting to the superior colliculus in new world monkeys. Anat Rec A Discov Mol Cell Evol Biol 285A:619–627.
Dorris MC, Paré M, Munoz DP (1997) Neuronal activity in monkey superior colliculus related to the initiation of saccadic eye movements. J Neurosci 17:8566–8579.
Douglas RJ, Martin KA (1991) A functional microcircuit for cat visual cortex. J Physiol 440:735–769.
Douglas RJ, Martin KAC (2004) Neuronal circuits of the neocortex. Annu Rev Neurosci 27:419–451.
Duhamel J-R, Colby CL, Goldberg ME (1992) The updating of the representation of visual space in parietal cortex by intended eye movements. Science 255:90–92.
Everling S, Munoz DP (2000) Neuronal correlates for preparatory set associated with pro-saccades and anti-saccades in the primate frontal eye field. J Neurosci 20:387–400.
Feizpour A, Majka P, Chaplin TA, Rowley D, Yu H-H, Zavitz E, Price NSC, Rosa MGP, Hagan MA (2021) Visual responses in the dorsolateral frontal cortex of marmoset monkeys. J Neurophysiol 125:296–304.
Ferraina S, Paré M, Wurtz RH (2002) Comparison of cortico-cortical and cortico-collicular signals for the generation of saccadic eye movements. J Neurophysiol 87:845–858.
Ghahremani M, Hutchison RM, Menon RS, Everling S (2017) Frontoparietal functional connectivity in the common marmoset. Cereb Cortex 27:3890–3905.
Ghahremani M, Johnston KD, Ma L, Hayrynen LK, Everling S (2019) Electrical microstimulation evokes saccades in posterior parietal cortex of common marmosets. J Neurophysiol 122:1765–1776.
Gnadt JW, Andersen RA (1988) Memory related motor planning activity in posterior parietal cortex of macaque. Exp Brain Res 70:216–220.
Godlove DC, Maier A, Woodman GF, Schall JD (2014) Microcircuitry of agranular frontal cortex: testing the generality of the canonical cortical microcircuit. J Neurosci 34:5355–5369.
Goldberg ME, Bisley J, Powell KD, Gottlieb J, Kusunoki M (2002) The role of the lateral intraparietal area of the monkey in the generation of saccades and visuospatial attention. Ann N Y Acad Sci 956:205–215.
Gottlieb J, Goldberg ME (1999) Activity of neurons in the lateral intraparietal area of the monkey during an antisaccade task. Nat Neurosci 2:906–912.
Green DM, Swets JA (1966) *Signal detection theory and psychophysics*. New York, NY: John Wiley.
Hanes DP, Schall JD (1996) Neural control of voluntary movement initiation. Science 274:427–430.
Hastie T, Tibshirani R (1986) Generalized additive models. Stat Sci 1:297–318.
Heinzle J, Hepp K, Martin KAC (2007) A microcircuit model of the frontal eye fields. J Neurosci 27:9341–9353.
Hussar CR, Pasternak T (2012) Memory-guided sensory comparisons in the prefrontal cortex: contribution of putative pyramidal cells and interneurons. J Neurosci 32:2747–2761.
Hwang J, Mitz AR, Murray EA (2019) NIMH MonkeyLogic: behavioral control and data acquisition in MATLAB. J Neurosci Methods 323:13–21.
Ipata AE, Gee AL, Goldberg ME, Bisley JW (2006) Activity in the lateral intraparietal area predicts the goal and latency of saccades in a free-viewing visual search task. J Neurosci 26:3656–3661.
Johnston KD, Barker K, Schaeffer L, Schaeffer DJ, Everling S (2018) Methods for chair restraint and training of the common marmoset on oculomotor tasks. J Neurophysiol 119:1636–1646.
Johnston KD, Everling S (2008) Neurophysiology and neuroanatomy of reflexive and voluntary saccades in non-human primates. Brain Cogn 68:271–283.
Jun JJ, et al. (2017) Fully integrated silicon probes for high-density recording of neural activity. Nature 551:232–236.
Karsh B. (2019). SpikeGLX: synchronized acquisition from imec neural probes and NI-DAQ devices (Version v20190413-phase3B2) [C]. Available at: https://github.com/billkarsh/SpikeGLX
Kusunoki M, Gottlieb J, Goldberg ME (2000) The lateral intraparietal area as a salience map: the representation of abrupt onset, stimulus motion, and task relevance. Vision Res 40:1459–1468.
Lewis JW, Van Essen DC (2000) Corticocortical connections of visual, sensorimotor, and multimodal processing areas in the parietal lobe of the macaque monkey. J Comp Neurol 428:112–137.
Lynch JC, Graybiel AM, Lobeck LJ (1985) The differential projection of two cytoarchitectonic subregions of the inferior parietal lobule of macaque upon the deep layers of the superior colliculus. J Comp Neurol 235:241–254.
Ma L, Selvanayagam J, Ghahremani M, Hayrynen LK, Johnston KD, Everling S (2020) Single-unit activity in marmoset posterior parietal cortex in a gap saccade task. J Neurophysiol 123:896–911.
Matsuzaki R, Kyuhou S, Matsuura-Nakao K, Gemba H (2004) Thalamo-cortical projections to the posterior parietal cortex in the monkey. Neurosci Lett 355:113–116.
McCormick DA, Connors BW, Lighthall JW, Prince DA (1985) Comparative electrophysiology of pyramidal and sparsely spiny stellate neurons of the neocortex. J Neurophysiol 54:782–806.
McDowell JE, Dyckman KA, Austin B, Clementz BA (2008) Neurophysiology and neuroanatomy of reflexive and volitional saccades: evidence from studies of humans. Brain Cogn 68:255–270.
McPeek RM, Keller EL (2002) Saccade target selection in the superior colliculus during a visual search task. J Neurophysiol 88:2019–2034.
Mendoza-Halliday D, et al. (2023) A ubiquitous spectrolaminar motif of local field potential power across the primate cortex (p. 2022.09.30.510398). bioRxiv.
Mirpour K, Arcizet F, Ong WS, Bisley JW (2009) Been there, seen that: a neural mechanism for performing efficient visual search. J Neurophysiol 102:3481–3491.
Mitchell JF, Sundberg KA, Reynolds JH (2007) Differential attention-dependent response modulation across cell classes in macaque visual area V4. Neuron 55:131–141.
Mitra PP, Pesaran B (1999) Analysis of dynamic brain imaging data. Biophys J 76:691–708.
Munuera J, Duhamel J-R (2020) The role of the posterior parietal cortex in saccadic error processing. Brain Struct Funct 225:763–784.
Nandy AS, Nassi JJ, Reynolds JH (2017) Laminar organization of attentional modulation in macaque visual area V4. Neuron 93:235–246.
Ninomiya T, Dougherty K, Godlove DC, Schall JD, Maier A (2015) Microcircuitry of agranular frontal cortex: contrasting laminar connectivity between occipital and frontal areas. J Neurophysiol 113:3242–3255.
Pachitariu M, Sridhar S, Stringer C (2023) Solving the spike sorting problem with Kilosort (p. 2023.01.07.523036). bioRxiv.
Paré M, Hanes DP (2003) Controlled movement processing: superior colliculus activity associated with countermanded saccades. J Neurosci 23:6480–6489.
Paxinos G, Charles W, Michael P, Rosa MGP, Hironobu T (2012) *The marmoset brain in stereotaxic coordinates*. San Diego, CA: Academic Press.
Pettine WW, Steinmetz NA, Moore T (2019) Laminar segregation of sensory coding and behavioral readout in macaque V4. Proc Natl Acad Sci U S A 116:14749–14754.
Reser DH, Burman KJ, Yu H-H, Chaplin TA, Richardson KE, Worthy KH, Rosa MGP (2013) Contrasting patterns of cortical input to architectural subdivisions of the area 8 complex: a retrograde tracing study in marmoset monkeys. Cereb Cortex 23:1901–1922.
Rosa MGP, Palmer SM, Gamberini M, Burman KJ, Yu H-H, Reser DH, Bourne JA, Tweedale R, Galletti C (2009) Connections of the dorsomedial visual area: pathways for early integration of dorsal and ventral streams in extrastriate cortex. J Neurosci 29:4548–4563.
Rossant C (2019) phy: interactive visualization and manual spike sorting of large-scale ephys data (2.0b1) [Python].
Schaeffer DJ, et al. (2022) An open access resource for functional brain connectivity from fully awake marmosets. NeuroImage 252:119030.
Schaeffer DJ, Gilbert KM, Hori Y, Hayrynen LK, Johnston KD, Gati JS, Menon RS, Everling S (2019) Task-based fMRI of a free-viewing visuosaccadic network in the marmoset monkey. NeuroImage 202:116147.
Schall JD (1995) Neural basis of saccade target selection. Rev Neurosci 6:63–85.
Selvanayagam J, Johnston KD, Schaeffer DJ, Hayrynen LK, Everling S (2019) Functional localization of the frontal eye fields in the common marmoset using microstimulation. J Neurosci 39:9197–9206.
Shen K, Valero J, Day GS, Paré M (2011) Investigating the role of the superior colliculus in active vision with the visual search paradigm. Eur J Neurosci 33:2003–2016.

Sommer MA, Wurtz RH (2004) What the brain stem tells the frontal cortex. I. Oculomotor signals sent from superior colliculus to frontal eye field via mediodorsal thalamus. J Neurophysiol 91:1381–1402.

Sommer MA, Wurtz RH (2006) Influence of the thalamus on spatial visual processing in frontal cortex. Nature 444:374–377.

Sommer MA, Wurtz RH (2008) Visual perception and corollary discharge. Perception 37:408–418.

Swadlow HA (2002) Thalamocortical control of feed-forward inhibition in awake somatosensory "barrel" cortex. J Neurophysiol 357:1717–1727.

Thomas NWD, Paré M (2007) Temporal processing of saccade targets in parietal cortex area LIP during visual search. J Neurophysiol 97: 942–947.

Thompson KG, Hanes DP, Bichot NP, Schall JD (1996) Perceptual and motor processing stages identified in the activity of macaque frontal eye field neurons during visual search. J Neurophysiol 76:4040–4055.

Wardak C, Olivier E, Duhamel J-R (2002) Saccadic target selection deficits after lateral intraparietal area inactivation in monkeys. J Neurosci 22: 9877–9884.

Westerberg JA, Sigworth EA, Schall JD, Maier A (2021) Pop-out search instigates beta-gated feature selectivity enhancement across V4 layers. Proc Natl Acad Sci U S A 118:e2103702118.

Wurtz RH, Sommer MA, Paré M, Ferraina S (2001) Signal transformations from cerebral cortex to superior colliculus for the generation of saccades. Vision Res 41:3399–3412.

Zhou Y, Liu Y, Lu H, Wu S, Zhang M (2016) Neuronal representation of saccadic error in macaque posterior parietal cortex (PPC). Elife 5: e10912.

Zhou Y, Liu Y, Wu S, Zhang M (2018) Neuronal representation of the saccadic timing signals in macaque lateral intraparietal area. Cereb Cortex 28: 2887–2900.